

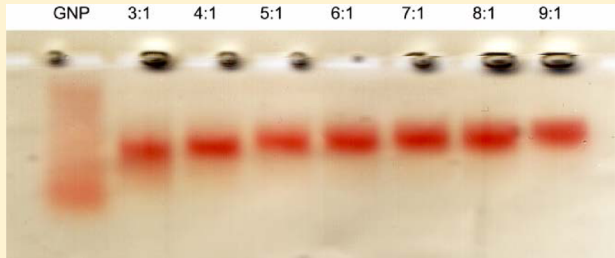
Quantifying the Association Constant and Stoichiometry of the Complexation between Colloidal Polyacrylate-Coated Gold Nanoparticles and Chymotrypsin

Jie Hou,[†] Diane M. Szaflarski,^{‡,*} and John D. Simon^{*,†,‡}

[†]Department of Chemistry, Duke University, Durham, North Carolina 27708, United States

[‡]Department of Chemistry, University of Virginia, Charlottesville, Virginia 22904, United States

ABSTRACT: Qualitative and quantitative insights into the capacity and association constant for the binding of chymotrypsin to polyacrylate-coated gold nanoparticles is determined using fluorescence quenching, optical absorption and circular dichroism spectroscopy, isothermal calorimetry, and gel electrophoresis. The collective data reveal a binding capacity and constant for this particular system of ~ 7 and $\sim 2 \times 10^6 \text{ M}^{-1}$, respectively. These values vary among the individual techniques, and not all techniques are able to provide quantitative information. The present study demonstrates that accurately quantifying the association between nanoparticles and biological materials requires using multiple approaches to ensure consistency among the binding parameters determined.



INTRODUCTION

Nanoparticles are now used pervasively in commercial products such as textiles, sunscreens, cosmetics, and agricultural pesticides.^{1–4} Numerous applications of nanoparticles in the health field are emerging, including antibacterial fabrics embedded with silver nanoparticles⁵ and surface modified particles designed for drug delivery.⁶ As a result, there is a tremendous interest in understanding the impact nanoparticle systems have on humans and the environment, and this interest is reflected by an increasing number of studies examining the toxicological impact of nanoparticles on cells and living organisms.^{7,8} It is not yet clear whether the disparate collection of nanoparticles being used in applications share common properties in terms of biological/environmental impact, or if the impact of each individual type of nanoparticles must be independently assessed.^{9,10} Many nanoparticles are effectively transported across cell membranes,¹¹ and so it is a central challenge to now unravel the action of nanoparticles on the cellular components and biomolecules.^{12–16} Only through such investigations can one understand the impact of nanoparticles on living systems and use that information to engineer and produce nanoparticles to mitigate any adverse effects.

The elucidation of general trends from the quantification of specific nanoparticle–protein complexes requires accurate determination of the thermodynamics of binding. As examples of features of nanoparticle–protein interactions, reports by Rotello and co-workers reveal insights into how binding to surface-modified gold nanoparticles that present amino acids to the coordinating protein affect the strength of protein binding and the effect of binding on the structure of the protein.^{17–20} Studies by Dawson and co-workers established the concept of a corona effect, reflecting that long-range interactions can result

in the formation of multiple layers of protein adsorption on the surface of a nanoparticle.^{21–23}

Several approaches are currently used to determine the capacity and binding constants for nanoparticle–proteins complexation. Herein, a detailed comparison between techniques on a single system is reported; such a study is necessary to assess the accuracy and limitations of any one technique. Most of the approaches used are borrowed from the field of ligand binding to proteins.²⁴ While ligand binding to proteins, and biomolecules binding to nanoparticles share some of the same features in this regard, they also have differences that must be taken into account in the analysis of data derived from such experiments. For example, because of the difference in size between nanoparticles and ligands and the fact that most nanoparticles are metals, the analysis of optical data must carefully account for scattering, metal-induced changes in molecular oscillator strengths, and inner-filter effects. The roles these factors play in affecting spectral information can be significantly different for metallic nanoparticles than for organic ligands. Agarose gel electrophoresis is used to quantify binding capacity, reflecting the fact that the size and surface charge of the complex is different from that of either the isolated nanoparticle or protein. In this case as well, one has to also address the possible interaction of the protein with the stabilizer molecules that are often present in commercial solutions of nanoparticles, molecules that would not be present

Special Issue: Paul F. Barbara Memorial Issue

Received: September 3, 2012

Revised: December 21, 2012

in ligand binding studies. Isothermal calorimetry (ITC) has been used to determine the binding constant and capacity of ligands to proteins.²⁵ The application of ITC to nanoparticles has been somewhat limited;^{16–23,26} but ITC shows great potential to contribute in this area. However, here as well, the thermodynamic parameters derived from ITC data are dependent on the specific binding model employed and the competitive equilibria that occur in the sample, and the data themselves do not always distinguish between possible models or enable unique extraction of one chemical process occurring in competition with others.

In the present paper, we discuss a single system—commercially available polyacrylate-coated gold nanoparticles and chymotrypsin—with the goal being to quantify the binding constant and stoichiometry. The work presented herein provides a comparison of the binding parameters determined by individual techniques, revealing the limitations and applicability of using specific approaches for quantifying protein/nanoparticle interactions.

■ EXPERIMENTAL SECTION

Materials. Carboxy-functionalized gold nanoparticle colloidal suspension (AuNP) was purchased from Vive Crop Protection (previously Vive Nano, Toronto, Canada). The nanoparticle suspension was used without further handling or purification. The stability of the suspension results from the fact that the solution is actually a colloid, in which excess polymer is present to stabilize the coated nanostructures, mitigating aggregation and precipitation. The functionalized nanoparticles have a polymer coating prepared by the collapsing of polyacrylate around the metal core.²⁷ The concentration is reported as 1.5 mg/mL. Taking the mean diameter of 4 nm, an average concentration of the nanoparticle stock solution used in the reported studies was 300 nM. Chymotrypsin (ChT) type II from bovine pancreas was purchased from Sigma-Aldrich. All the solutions were prepared in ultrapure water (>18.2 MΩ, Millipore, Billerica, USA).

Transmission Electron Microscopy (TEM). The size of the samples were characterized using an FEI Tecnai G2 20 TWIN instrument. The samples were taken using two 2 μL portions of a 0.3 μM AuNP solution. One droplet was placed on the TEM grid. The grid was whisked (liquid was removed with the side of a kimwipe) and allowed to dry in the dark. A second droplet was then added, whisked, allowed to dry, and the TEM images were taken of the product.

Gel Electrophoresis. All the samples and agarose gels were prepared in 5 mM sodium phosphate buffer (pH 7.4). After incubating for 2 h, the mixtures of AuNP (0.27 μM) and varying concentrations of ChT (ChT:AuNP ratios from 3:1 to 9:1) were separated by 1% agarose gel electrophoresis at 100 V for 20 min.

Optical Spectroscopy. All spectra were collected at room temperature, unless otherwise specified. The samples were prepared in sodium phosphate buffer, at pH 7.4. UV-visible absorption spectra were recorded using a Varian Cary 50 Bio UV-vis spectrophotometer. The UV CD spectra were measured on an Aviv model 202 CD spectrophotometer. The static fluorescence spectra were collected using a Fluorolog 3 Fluorometer (Horiba Jobin-Yvon, Edison, NJ, USA). A 1 cm quartz cell was used to collect the emission spectra from 305 to 450 nm, using an excitation wavelength of 295 nm. Time-resolved emission decays were collected using a PicoQuant Fluoro100, exciting the sample at 289 nm using a pulsed LED,

and collecting the total emission. A glass filter was inserted in front of the detector to minimize the Raleigh scattering of the incident light. FluoFit Software was used to fit the time-resolved spectra.

Isothermal Titration Calorimetry (ITC). ITC experiments were carried out on a VP-ITC ultrasensitive microcalorimeter (Microcal, Northampton, MA) at 25 °C. During the titration, 40 successive injections of a constant volume (7 μL/injection) of ChT solutions (30 μM) were injected into a reaction cell (1.46 mL) filled with a AuNP solution (0.27 μM). Both the ChT and AuNP solutions were prepared in 5 mM phosphate buffer, pH 7.4. All solutions were degassed for 10 min prior to the titrations to avoid the formation of bubbles in the sample cell. Microcal Origin software (version 7.0) was used to fit ITC titration data curve, from which the stoichiometry (*n*), equilibrium binding constant (*K_b*), and enthalpy of complex formation (Δ*H*) were determined.

■ RESULTS AND DISCUSSION

TEM. The size distribution of the AuNP samples was examined by TEM imaging (Figure 1). The dark features in the

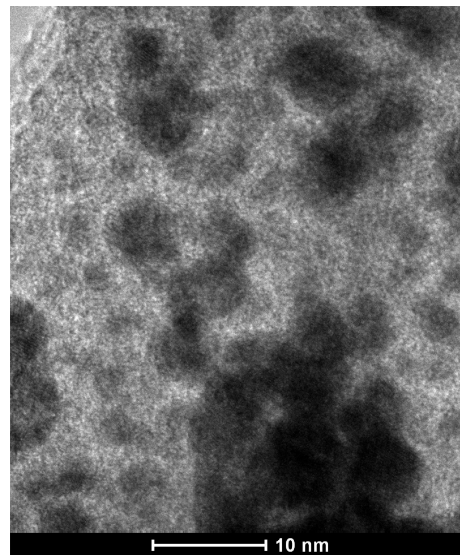


Figure 1. TEM of carboxy-functionalized AuNPs from Vive Crop Protection. The dark regions indicate the Au core, reflecting a size distribution of ~2–6 nm. The core is surrounded by a ~2 nm polyacrylate coating. The free polyacrylate in the solution, which acts as a stabilizer for the nanoparticles, can also be observed as a surface coating in the image.

image are the Au core, reflecting particle diameters ranging from 2 to 6 nm, consistent with the manufacturer specifications. The image also reveals polymer material, coating the AuNPs, and the polyacrylate deposits, reflecting the presence of free polymer in the solution. The image suggests that the thickness of the polymer coating is ~2 nm.

Agarose Gel Electrophoresis. To establish binding between AuNP and ChT, agarose gel electrophoresis was carried out for protein:nanoparticle ratios ranging from 3:1 to 9:1 at a fixed concentration of AuNP of 270 nM; the results are shown in Figure 2. The AuNP band is clearly visible in the gel. The control lane containing AuNP indicates a broad distribution of nanoparticle sizes, with greater mobility being seen in the presence of protein. For a constant thickness of the

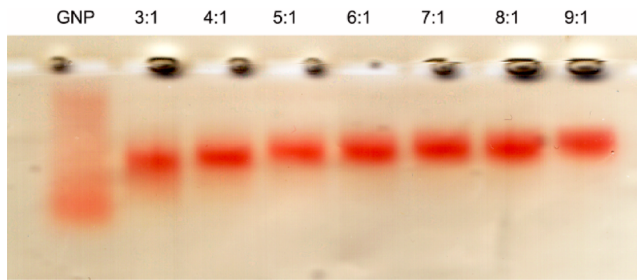


Figure 2. Agarose gel electrophoresis of the AuNPs ($0.27 \mu\text{M}$) as a function of ChT concentration. The ChT:AuNP ratio is varied from 0 to 9:1. The mobility of the AuNP is decreased by added protein (resulting from binding), but levels off between ~7–9:1, reflective of the binding stoichiometry.

polymer coating, an increase in the metal core diameter will result in an increased surface area and corresponding charge on the surface. The mobility, u , of a charged colloid particle of radius r can be calculated from the zeta potential, ζ , using Henry's formula:²⁸

$$u = 2\epsilon\zeta/3\eta f(kr) \quad (1)$$

where $f(kr) = 1 + (1/2)(1 + \delta/kr)^3$ with $\delta = 2.5/(1 + 2e^{-kr})$. The quantity $1/\kappa$ is the Debye length. The addition of a protein layer through association with the surface of the nanoparticle changes both the radius of the particle and ζ . Studies on the effect of poly(ethylene glycol) (PEG) layers on gold and silver nanoparticles clearly show that coatings of the nanoparticles can significantly affect mobility.²⁸ In addition, ionic strength and the presence of macromolecular ions can alter mobility. The Debye length is related to the concentrations of charged species in solution and hence will vary as the protein concentration is increased (ChT is a positively charged protein). As a result, following saturation of the ChT binding to the AuNP, additional protein will affect the Debye length and hence the mobility of the complex. Specifically, the mobility will decrease with increased protein concentration, and so the AuNP band will continue to shift even though the actual size and charge of the complex is unchanged. The effect of added protein on the mobility of the AuNP levels off for a protein:nanoparticle ratio of around 9:1. These results establish that ChT binds to these surface-modified AuNPs. Taking into account the range of size of the NPs and the fact that with increasing NP diameter, a larger number of proteins can, in principle, be coordinated to the NP surface, the gel data suggests a maximum binding stoichiometry of the ChT:AuNP complex is in the range of 7–9:1.

Optical Absorption Spectroscopy. The absorption spectra of AuNP and ChT at concentrations of 21 nM and $1.07 \mu\text{M}$, respectively, in 5 mM sodium phosphate buffer (pH 7.4) were examined. ChT shows an absorption maximum at 295 nm, reflective of its aromatic amino acid content. The AuNPs are characterized by a broad plasmon band at 520 nm, which sits on top of a broad continuous absorption extending from approximately 750 nm into the UV. The absorption spectrum of the mixture is indistinguishable from that for the sum of the constituents, indicating that under these conditions, no changes in the electronic absorption properties of the system can be observed. If we assume a binding stoichiometry of 7:1 (the lower limit implied by the gel data above), then at most $\sim 0.15 \mu\text{M}$ of the protein would be bound, or $\sim 14\%$ of the protein in the solution. With such a small fraction of the protein

bound, changes in the bulk protein absorption may be difficult to distinguish. However, under these conditions, all of the nanoparticles in solution would be coated in protein, and so we can conclude that binding has no observable effect on the plasmon band. Analyses of the optical absorption spectra alone do not provide insight into protein–nanoparticle binding for this system.

Circular Dichroism (CD) Spectroscopy. Ultraviolet CD spectroscopy can provide more insights than simple absorption spectroscopy, as it is sensitive to changes in the secondary structure of the protein. Figure 3 shows the CD spectra for

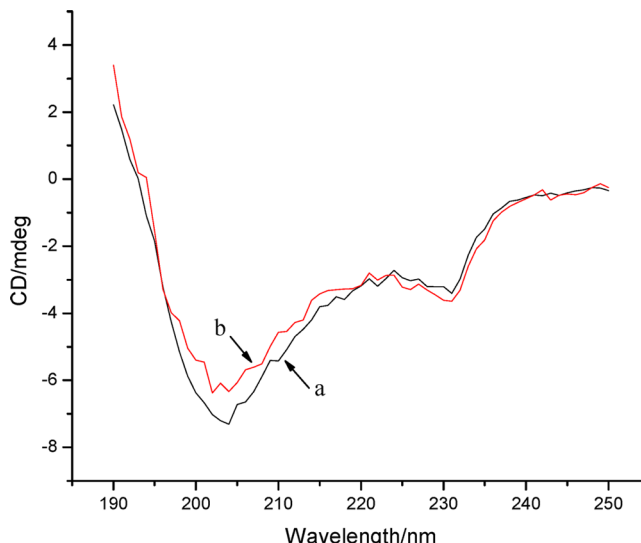


Figure 3. The CD spectra of ChT ($4.4 \mu\text{M}$) in the absence (a) and presence (b) of a AuNP (270 nM) in 5 mM sodium phosphate buffer (pH 7.4) is shown. There is a small change in the CD spectrum in the region ~ 202 nm, reflective of a loss of α -helical structure in the presence of the AuNP.

ChT ($4.4 \mu\text{M}$, 5 mM sodium phosphate buffer, pH 7.4) and the effect of adding 270 nM AuNP. Once again, if we assume a binding stoichiometry of 7:1, $\sim 40\%$ of the protein in the solution would be bound to the nanoparticles.

The CD spectrum of ChT is similar to that reported elsewhere.²⁹ Upon addition of nanoparticles, there is a small decrease in the intensity of the CD band at 202 nm; the band at 231 is unaffected. The 202 nm band is reflective of α -helical structures; β -sheet and random coil structures have nearly no CD signals at this wavelength.^{30,31} The secondary structure of ChT consists of $\sim 15\%$ α -helix, so the data in Figure 3 suggest that the amount of α -helix decreases when the protein binds to the AuNP. Unlike the absorption data, the CD data do indicate that binding occurs.

Steady-State and Time-Resolved Fluorescence. The excitation of ChT at ~ 290 nm results in fluorescence, emanating from one or more of the four tryptophan residues in the protein. The fluorescence spectra for $1.0 \mu\text{M}$ ChT solutions containing varying concentrations of AuNP (maximum of 180 nM) are presented in Figure 4. The fluorescence decreases with increasing AuNP:ChT ratio. At a AuNP:ChT ratio of $\sim 1:5$, the fluorescence decreases by $\sim 90\%$ compared to that of the protein alone. These data suggest that complex formation between ChT and AuNPs results in the quenching of the protein emission. In principle, such fluorescence quenching data can be used to quantify the binding constant. However,

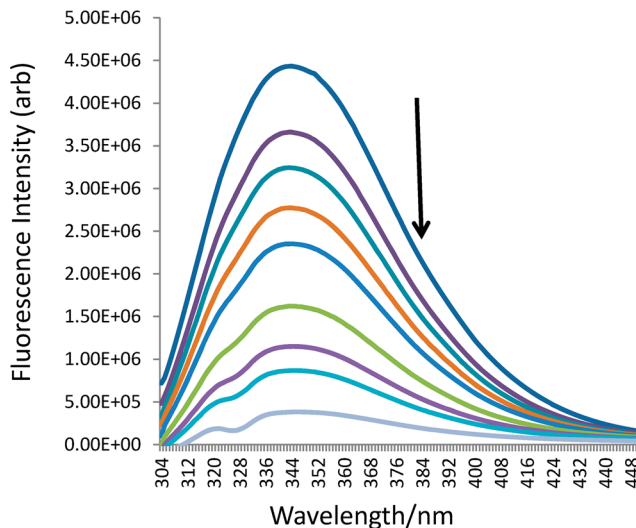


Figure 4. Fluorescence spectra of 1.0 μM ChT excited at 295 nm are shown as a function of added AuNP. The AuNP concentration is increased from 0 nM to 240 nM, and the fluorescence is quenched. The data show that $\sim 90\%$ of the fluorescence is quenched at a ChT:AuNP ratio of $\sim 5:1$. The arrow indicates that the fluorescence decreases with increased concentration of nanoparticles.

this requires relating the fluorescence intensity to the concentration of free protein in solution. In the present experiments, it is important to realize that the AuNPs absorb at both the excitation wavelength used to generate the fluorescence and in the region of the protein emission. Thus, as the AuNP concentration is changed for a fixed concentration of protein, not only is the concentration of free and complexed protein altered, but the transmission of the excitation and emission light through the sample is affected. The AuNPs therefore act as an inner-filter, and this must be taken into account in analyzing the emission intensity data. The emission intensity can be corrected for this inner-filter effect^{32–34} using

$$I_{\text{corr}} = I_{\text{meas}} \beta_{\text{ab}} \beta_{\text{em}} \quad (2)$$

where

$$\beta = \exp\left(\frac{\alpha(\lambda_i)L_i}{2}\right) \times \left(\frac{\left(\frac{\alpha(\lambda_i)\Delta_i}{2}\right)}{\sinh\left(\frac{\alpha(\lambda_i)\Delta_i}{2}\right)} \right) \quad (3)$$

In the above expression, $\alpha(\lambda_i)$ is the absorption coefficient at λ_i , Δ_i is the detection volume, and L_i is the length light travels in the cell.

It is instructive to compare the results obtained with and without taking the inner-filter effect into account. Specifically, using the emission spectra reported in Figure 4, the fluorescence intensity at 355 nm, with and without the inner-filter correction, is plotted in Figure 5 as a function of AuNP concentration. The intensity profiles are clearly different, and therefore any model used to extract quantitative information about the binding from fluorescence data will give erroneous results if the inner-filter effect is not accounted for.

One common approach for determining the association constant from fluorescence quenching data is to use the Stern–Volmer equation.^{24,33–37} This analysis is can be used to describe two different processes: static and dynamic quenching. In the case of static quenching (e.g., a stable complex is formed

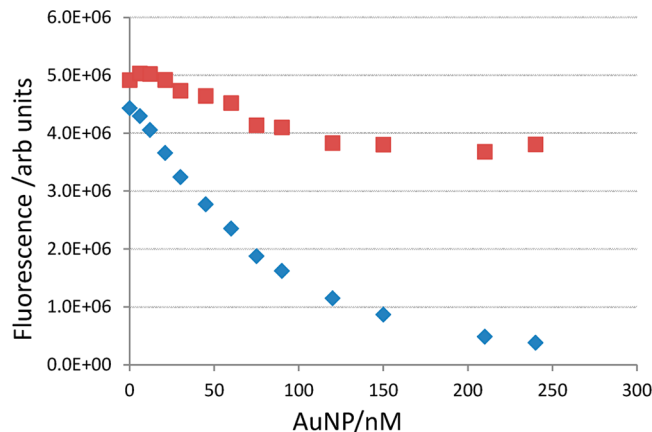


Figure 5. The intensity of the fluorescence at 355 nm (Figure 4) is plotted as a function of the concentration of added AuNP (◆). The same data corrected for the inner-filter effect is also plotted (■). The corrected data show that the actual fluorescence quenching is significantly less than that implied by the collected data, reflecting the large inner-filter effect caused by changing the nanoparticle concentration.

between the NP and protein), the ratio of the fluorescence in the absence of the NP, F_0 , to that at a certain NP concentration, F , is given by

$$F_0/F = 1 + K_{\text{SV}}[\text{AuNP}] \quad (4)$$

where K_{SV} is the Stern–Volmer constant. In the limit of static quenching, K_{SV} is the thermodynamic association constant, K_a . In the limit of dynamic quenching, $K_{\text{SV}} = k_q \tau_0$, where k_q is the bimolecular quenching rate constant, and τ_0 is the average fluorescence lifetime. (This model assumes a 1:1 binding stoichiometry.)

If both static and dynamic quenching occur, then

$$F_0/F = (1 + k\tau_0[\text{AuNP}]) (1 + K_a[\text{AuNP}]) \quad (5)$$

and a plot of F_0/F vs [AuNP] will exhibit a positive quadratic shape. Examining Figure 6, the data uncorrected for the inner-filter effect exhibits such quadratic curvature, from which one would conclude that the fluorescence data reflects both static and dynamic quenching processes.

However, if one were to make such a conclusion, a fit to these data gives $k\tau_0 K_a = 0.0002$ and $k\tau_0 + K_a = 0.029$, for which there is no real solution for K_a . However, the fluorescence intensity data corrected for the inner filter effect is linearly dependent on the concentration of AuNPs, and the best fit of eq 4 to this data gives $K_{\text{SV}} = 1.6 \times 10^6 \text{ M}^{-1}$. The quenching of the fluorescence is dominated by (or exclusively arises from) either a static or dynamic process, not both. The agarose gel data presented above indicates the formation of stable complexes, which would suggest that the fluorescence quenching results from a static mechanism, in which case K_{SV} would be the thermodynamic binding constant.

In order to unambiguously determine whether the quenching is dynamic or static, time-resolved fluorescence decays were recorded for a constant concentration of ChT (200 nM) in the presence of an increasing concentration of AuNP (up to ~ 40 nM). Similar to the steady-state data, the integrated intensity of the time-resolved fluorescence decay decreases with increasing concentration of AuNP (see Figure 7). ChT in the absence of AuNP is best described by a triexponential decay. The fluorescence lifetimes extracted from these data using were

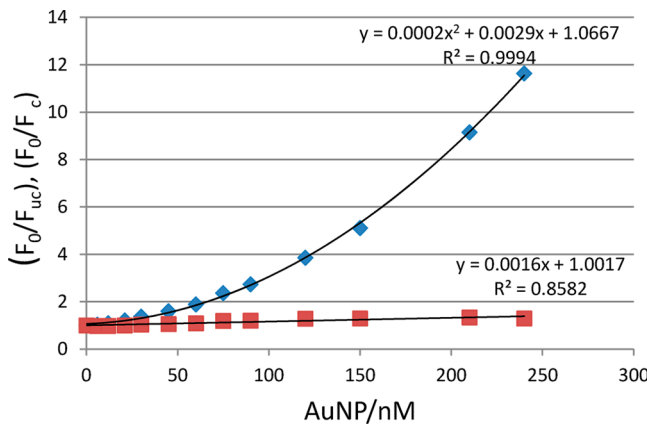


Figure 6. Stern–Volmer analysis of the fluorescence intensity data presented in Figure 5. The data corrected for the inner filter effect (F_0/F_c ; ■) exhibits a linear dependence on concentration, whereas the uncorrected data (F_0/F_{uc} ; ◆) shows quadratic behavior. These would lead to different interpretations, reflecting the need to correct the data to take into account inner-filter effects in order to derive accurate binding information from fluorescence data. The results of a linear and quadratic regression fit (see eqs 4 and 5) to F_0/F_c and F_0/F_{uc} , respectively, are given in the figure.

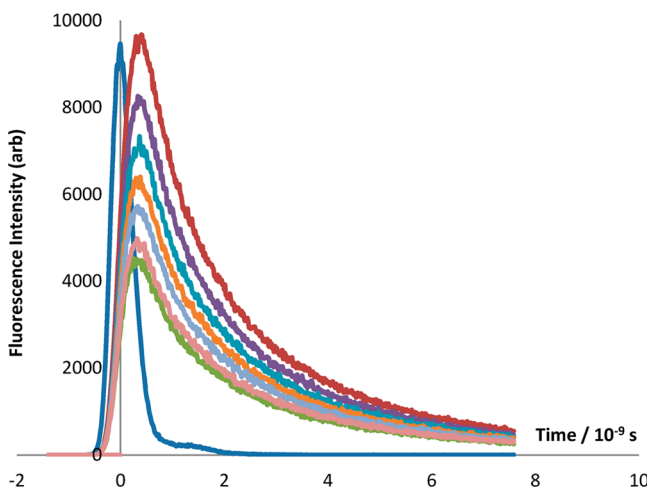


Figure 7. Time-resolved emission decays of the fluorescence of 200 nM ChT as a function of added AuNP. The maximum concentration of added AuNP was 40 nm, or a ChT:AuNP ratio of 5:1. At this ratio, the fluorescence intensity is ~50% of that in the absence of nanoparticles. Added AuNP quenches the emission (as observed in the steady state spectra, Figure 4), but the time-resolved data show that the shape of the decay is independent of added nanoparticles. This establishes that quenching occurs by a static model, in which case the Stern–Volmer constant is a measure of the binding constant between the protein and nanoparticles.

4.01, 1.71, and 0.59 ns, which are in excellent agreement with previous reports.^{38,39} In the presence of AuNP, the integrated intensity under the decay curve decreases—consistent with the steady state spectra—but the decay times and their relative amplitudes are unaffected by the added nanoparticles. These data clearly rule out any contribution from dynamic quenching, and so the Stern–Volmer constant determined above is the thermodynamic association constant, $K_a = 1.6 \times 10^6 \text{ M}^{-1}$.

There are other models in addition to a Stern–Volmer analysis for extracting binding parameters from fluorescence quenching data. If we consider the case where the nanoparticles

have n equivalent and noninteracting binding sites, each characterized then by the same equilibrium constant K , then r , the ratio of the concentration of bound protein to total concentration of binding sites, is expressed by the following rectangular hyperbolic function:⁴⁰

$$r = nK_a c / (1 + K_a c) \quad (6)$$

where c is the concentration of free protein. To determine n and K from the equilibrium binding curve requires collecting data over a wide range of values of c , which in the case of protein association with nanoparticles is not easily performed due to the solubility properties of proteins and protein aggregation effects. As a result, it is common to use linear transforms of eq 6 to determine these parameters, and one commonly used form to determine binding affinity constants is the Skatchard equation:²⁴

$$r/c = nK_a - rK_a \quad (7)$$

To use this equation to treat nanoparticles requires independent determination of n , as r is given by the product $n[\text{AuNP}]$. If one assumes a binding capacity of 7–9 (from the gel data) so that r can be calculated and then performs this analysis on the inner-filter corrected integrated intensities of the fluorescence decays, one obtains $K_a = 4 \times 10^6 \text{ M}^{-1}$ and $n = 3\text{--}4$. If we set the binding capacity to be $n = 3$ to calculate r , then the Skatchard analysis returns a value of $n = 2.5$, consistent with the original assumption, suggesting that the stoichiometry is ~3:1. It remains the case that a limited set of (r, c) data can be deduced from fluorescence quenching experiments, and so the Skatchard analysis provides estimates of n and K_a , and the data set is too limited to carry out a full nonlinear analysis using eq 6. This is commonly the case in many systems, and especially so in the analysis of protein binding to nanoparticles, but is often overlooked in the application of the data analysis.

The two models explored—Stern Volmer and Skatchard—assume details related to the stoichiometry and/or the mechanism. Stern–Volmer analysis assumes $n = 1$, and, in the case of the Skatchard analysis, that there are n -independent noninteracting binding sites. While this may be the case, there is no independent experimental evidence supporting this assumption. These are, however, the simplest models, and if the data can be well described by the mathematics of such a model, then surely a more complicated model with additional parameters could also generate excellent fits. As mentioned above, determination of n and K_a from fluorescence quenching requires data covering an extensive concentration range so that the shape of the equilibrium binding curve is established, which in the case of protein association with nanoparticles generally cannot be collected due to the solubility properties of proteins and protein aggregation effects.

ITC. Figure 8 presents the results of an ITC titration of ChT (30 μM) into a 270 nM solution of AuNP. The data were modeled assuming that the AuNP is characterized by a single set of equivalent and noninteracting binding sites. The fit to the data, also shown, gives a binding capacity and binding constant of $n = 5.5$ and $K_a = 9.6 \times 10^5 \text{ M}^{-1}$, respectively.

ITC gives direct insight in binding strength and capacity, yet, like all of the techniques explored, requires the use of a thermodynamic model, which can range from assuming a single set of equivalent and noninteracting binding sites (used in the reported analysis), to multiple sets of sites of varying capacity and binding strength.

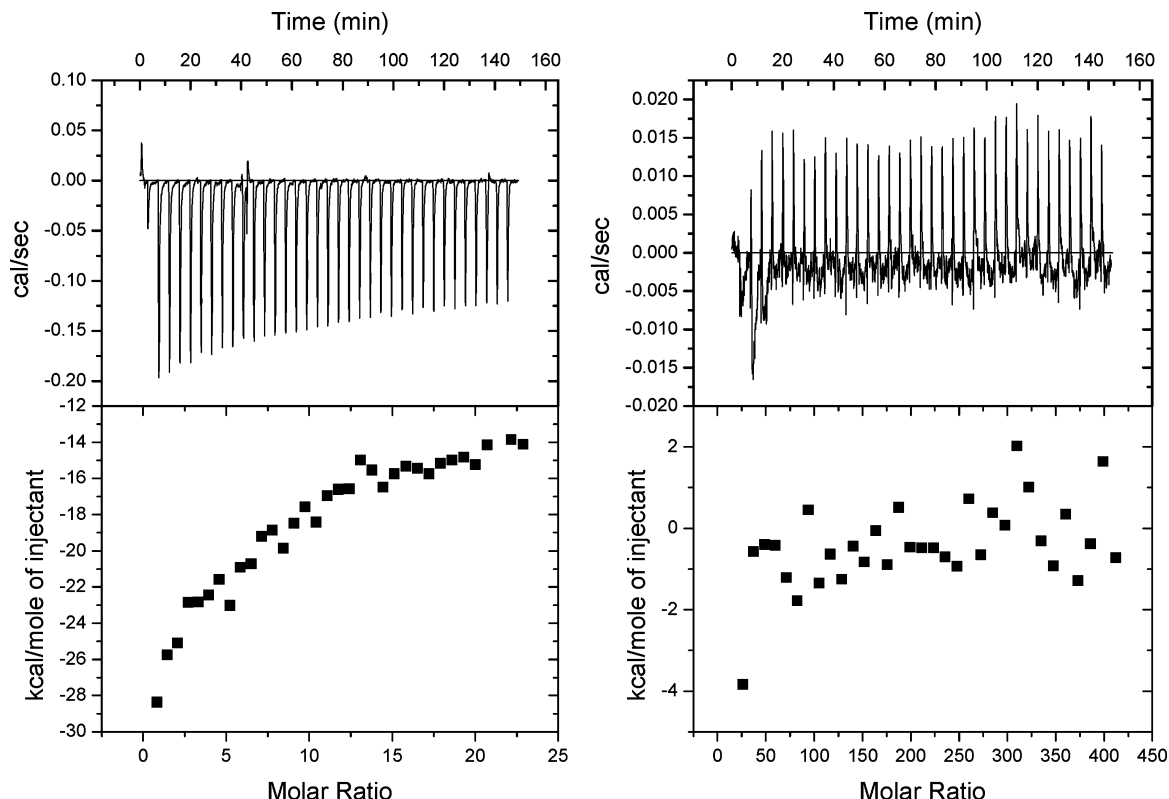


Figure 8. ITC data for the titration of ChT ($30\ \mu\text{M}$) into (left) $270\ \text{nM}$ GNP and (right) $5\ \text{mM}$ sodium phosphate buffer. All the reactants are also present in $5\ \text{mM}$ sodium phosphate buffer. The data is well described by a model assuming n equivalent and noninteracting binding sites with a binding stoichiometry of $5.5\ \text{ChT}/\text{AuNP}$ and binding constant of $9.6 \times 10^5\ \text{M}^{-1}$.

Table 1 presents the comparative data on the quantitative binding constants and stoichiometry derived from the

Table 1. Summary of Binding Constants, K , and Stoichiometry, n^a

technique	n	K
agarose gel	7–9/1	
Stern–Volmer steady-state fluorescence		$1.6\ (\pm 0.3) \times 10^6\ \text{M}^{-1}$
Skatchard time-resolved fluorescence	~3	$4.0\ (\pm 0.6) \times 10^6\ \text{M}^{-1}$
ITC	~5.5	$9.6\ (\pm 0.2) \times 10^5\ \text{M}^{-1}$

^aThe errors are estimated to be on the order of 15%.

experimental approaches described above. Each technique—gel electrophoresis, fluorescence quenching, and ITC—provides quantitative information. However, each is *limited* by the need to assume a model in order to extract quantitative binding parameters from the measured data. For this particular system, the binding parameters derived from the data associated with the different experimental approaches are reasonably consistent with one another, but, collectively, the study highlights the challenges in determining accurate and precise measurements for the association of proteins with coated nanoparticles.

It is important to point out that one cannot use these results to clearly state which technique is the most reliable. While the approaches used differ in precision, the fact that the parameters are model-dependent suggests that accurate determination of protein–nanoparticle binding *must* involve validating consistency among a set of experimental approaches. Take, for example, the two approaches reported in this study that assume

the same underlying model; the ITC analysis and the Skatchard analysis of the fluorescence quenching. Both assume the existence of n equivalent and noninteracting binding sites on the surface of the nanoparticle. In both cases, the nanoparticles are assumed to be identical, but the TEM image in Figure 1 clearly reveals a size distribution. The binding capacity will likely differ across this size distribution, and effect that is not accounted for in any of the analyses. Taking the thickness of the coating to be 2 nm, and the distribution of the core radii as 1–3 nm (see TEM discussion above), the distribution in the radii of the coated nanoparticles would span from 3 to 5 nm. The larger particles would then have a surface area that is ~2.8 greater than that of the smallest particles. Given that the Stokes radius of chymotrypsin is ~2.1 nm,⁴¹ this would suggest that the binding capacity changes significantly over the size range of the particles present in solution.

From an ITC analysis, Dawson and co-workers concluded that the curvature of the surface plays an important role in the binding.²³ This could be important in the present study given the range in particle size. Specifically, Dawson and co-workers conjectured that a lower degree of surface coverage observed for smaller particles likely resulted from the fact that higher curvatures inhibited effective binding, and that the packing of proteins on the surface becomes more problematic as the radius of curvature of the particle becomes comparable to that of the protein. For a sphere, the Gaussian curvature varies as $1/r^2$, so similar to the surface area, the particles studied herein would exhibit a ~2.8 fold difference in the surface curvature over the size range present in solution. In addition, the smaller particles are comparable in size to chymotrypsin, and thus may not effectively participate in binding to the protein. In spite of these

underlying issues, Table 1 reveals that the determination of n and K_a from the Skatchard analysis and ITC data are similar in magnitude. The fact that the data can be described to a single type of binding site may reflect the fact that the observed binding is reflective of only a subset of the different size nanoparticles present.

AUTHOR INFORMATION

Corresponding Author

*E-mail: dms2fw@virginia.edu (D.M.S.); john.simon@virginia.edu (J.D.S.).

Notes

The authors declare no competing financial interest.

ACKNOWLEDGMENTS

We wish to acknowledge Duke University for support. We thank Ms. Keely Glass for providing the TEM image.

REFERENCES

- (1) Hamilton, T. *Can. Chem. News* **2012**, 12–15.
- (2) Smijs, T. G.; Pavel, S. *Nanotechnol., Sci. Appl.* **2011**, 4, 95–112.
- (3) Wiechers, J. W.; Musee, N. *J. Biomed. Nanotechnol.* **2010**, 6, 408–431.
- (4) Wang, S. Q.; Balagula, Y.; Osterwalder, U. *Dermatol. Ther.* **2010**, 23, 31–47.
- (5) Lee, H. Y.; Park, H. K.; Lee, Y. M.; Kim, K.; Park, S. B. *Chem. Commun.* **2007**, 28, 2959–2961.
- (6) Gupta, A. K.; Wells, S. *IEEE Nanobiosci.* **2009**, 3, 66–73.
- (7) Tran, D.; Salmon, R. *Australas. J. Dermatol.* **2010**, 52, 1–6.
- (8) El-Ansary, A.; Al-Daihan, S. J. *Toxicol.* **2009**, 754810.
- (9) Auffan, M.; Rose, J.; Bottero, J.-Y.; Lowry, G. V.; Jolivet, J.-P.; Wiesner, M. R. *Nat. Nanotechnol.* **2009**, 4, 634–641.
- (10) Zhang, H.; Ji, Z.; Xia, T.; Meng, H.; Low-Kam, C.; Liu, R.; Pokhrel, S.; Lin, S.; Wang, X.; Liao, Y.-P.; Wang, M.; et al. *ACS Nano* **2012**, 6, 4349–4368.
- (11) Chithrani, B. D.; Chan, W. C. *Nano Lett.* **2007**, 7, 1542–1550.
- (12) Rana, S.; Yeh, Y.-C.; Rotello, V. M. *Curr. Opin. Chem. Biol.* **2010**, 14, 828–834.
- (13) Lynch, I.; Cedervall, T.; Lundqvist, M.; Cabaleiro-Lago, C.; Linse, S.; Dawson, K. A. *Adv. Colloid Interface Sci.* **2007**, 134–135, 167–174.
- (14) De Paoli Lacerda, S. H.; Park, J. J.; Meuse, C.; Pristinski, D.; Becker, M. L.; Karim, A.; Douglas, J. F. *ACS Nano* **2010**, 4, 365–379.
- (15) Aubin-Ta, M. E.; Hamad-Schifferli, K. H. *Biomed. Mater.* **2008**, 3, 034001.
- (16) Lynch, I.; Dawson, K. A. *Nanotoday* **2008**, 3, 40–47.
- (17) You, C.-C.; De, M.; Rotello, V. M. *Org. Lett.* **2005**, 7, 5685–5688.
- (18) Fischer, N. O.; Verma, A.; Goodman, C. M.; Simard, J. M.; Rotello, V. M. *J. Am. Chem. Soc.* **2003**, 125, 13387–13391.
- (19) You, C.-C.; De, M.; Han, G.; Rotello, V. M. *J. Am. Chem. Soc.* **2005**, 127, 12873–12881.
- (20) De, M.; You, C.-C.; Srivastava, S.; Rotello, V. M. *J. Am. Chem. Soc.* **2007**, 129, 10747–10753.
- (21) Lindman, S.; Lynch, I.; Thulin, E.; Nilsson, H.; Dawson, K. A.; Linse, S. *Nano Lett.* **2007**, 7, 914–920.
- (22) Lundqvist, M.; Stigler, J.; Elia, G.; Lynch, I.; Cedervall, T.; Dawson, K. A. *Proc. Natl. Acad. Sci. U.S.A.* **2008**, 105, 14265–14270.
- (23) Cedervall, T.; Lynch, I.; Lindman, S.; Berggard, T.; Thulin, E.; Nilsson, H.; Dawson, K. A.; Linse, S. *Proc. Natl. Acad. Sci. U.S.A.* **2007**, 104, 2050–2055.
- (24) Dill, K.; Bromber, S. *Molecular Driving Forces: Statistical Thermodynamics in Chemistry & Biology*, 2nd ed.; Garland Science: New York, 2010.
- (25) Saboury, A. A. *J. Iran. Chem. Soc.* **2006**, 3, 1–21.
- (26) Asadi, A.; Saboury, A. A.; Moosavie-Movahedi, A. A.; Divsalar, A.; Sarbolouki, M. N. *Int. J. Biol. Macromol.* **2008**, 43, 262–270.
- (27) Goh, C. M.; Dinglasan, J. A.; Goh, J. B.; Loo, R.; Veletanlic, E., U.S. Patent 7,534,490 B1, May 19 2009.
- (28) Doane, T. L.; Cheng, Y.; Babar, A.; Hill, R. J.; Burda, C. *J. Am. Chem. Soc.* **2010**, 132, 15624–15631.
- (29) Morrisett, J. D.; Broomfield, C. A. *J. Am. Chem. Soc.* **1971**, 93, 7294–7304.
- (30) Cantor, R.; Schimmel, P. R. *Biophysical Chemistry Part II: Techniques for the Study of Biological Structure and Function*; W. H. Freeman & Co.: New York, 1980.
- (31) Hennessey, J. P.; Johnson, W. C. *Biochemistry* **1981**, 20, 1085–1094.
- (32) Van der Weert, M. *J. Fluoresc.* **2010**, 20, 625–629.
- (33) Zhao, X.; Liu, R.; Chi, Z.; Teng, Y.; Qin, P. *J. Phys. Chem. B* **2010**, 114, 5625–5631.
- (34) Lakowicz, J. *Principles of Fluorescence Spectroscopy*, 3rd ed.; Springer: New York, 2006.
- (35) Togashi, D. M.; Ryder, A. G.; McMahon, D.; Dunne, P.; McManus, J. *Proc. SPIE – Biomed. Opt.* **2007**, 6628, 66281.
- (36) Zolghadri, S.; Saboury, A. A.; Golestani, A.; Divsalar, A.; Rezaei-Zarchi, S.; Moosavi-Movahedi, A. A. *J. Nanopart. Res.* **2009**, 11, 1751–1758.
- (37) Pramanik, S.; Banerjee, P.; Sarker, A.; Bhattacharya, S. C. *J. Lumin.* **2009**, 128, 196901974.
- (38) Desei, G.; Boens, M.; van der Zegel, M.; de Schryver, S. *Anal. Chim. Acta* **1985**, 170, 45–59.
- (39) Vermunft, G.; Boens, M.; de Schryver, S. *Photochem. Photobiol.* **1991**, 53, 57–63.
- (40) Sawyer, W. H.; Winzor, D. J. *Curr. Protoc. Protein Sci.* **1999**, A.5A.1–A.5A.40.
- (41) Boulanger, R. R., Jr.; Kantrowitz, E. R. *J. Biol. Chem.* **2003**, 278, 23497–23501.